Vibration isolation design for periodically stiffened shells by the wave finite element method

Jie Hong [a, b], Xueqing He [a], Dayi Zhang [a, *], Bing Zhang [c], Yanhong Ma [a, b]

[a] School of Energy and Power Engineering, Beihang University, Beijing, 100191, PR China
[b] Collaborative Innovation Center of Advanced Aero-Engine, Beihang University, Beijing, 100083, PR China
[c] Rolls Royce Composites University Technology Centre (UTC), Bristol Composites Institute (ACCIS), University of Bristol, Queen's Building, University Walk, Bristol, BS8 1TR, UK

ARTICLE INFO

ABSTRACT

Periodically stiffened shell structures are widely used due to their excellent specific strength, in particular for aeronautical and astronautical components. This paper presents an improved Wave Finite Element Method (FEM) that can be employed to predict the band-gap characteristics of stiffened shell structures efficiently. An aero-engine casing, which is a typical periodically stiffened shell structure, was employed to verify the validation and efficiency of the Wave FEM. Good agreement has been found between the Wave FEM and the classical FEM for different boundary conditions. One effective wave selection method based on the Wave FEM has thus been put forward to filter the radial modes of a shell structure. Furthermore, an optimisation strategy by the combination of the Wave FEM and genetic algorithm was presented for periodically stiffened shell structures. The optimal out-of-plane band gap and the mass of the whole structure can be achieved by the optimisation strategy under an aerodynamic load. Results also indicate that geometric parameters of stiffeners can be properly selected that the out-of-plane vibration attenuates significantly in the frequency band of interest. This study can provide valuable references for designing the band gaps of vibration isolation.

1. Introduction

Thin shell structures have been widely used to reduce weight for modern mechanical systems, in particular for aeronautical and astronautical components Stiffeners are usually employed to improve the mechanical behaviour of thin shell structures, via forming a higher specific-strength structure, however, a stiffened shell structure is still susceptible to vibration. It is always difficult to suppress vibration due to natural modes inherent to the structure, in particular in the high frequency range. In engineering applications, the intense resonance may occur due to vibration and lead to severe hazards to machines [1–3].

In recent decades, a considerable amount of studies have been reported on the vibration control of periodic structures based on their band-gap properties. Due to the spatial periodicity, a "filtering" phenomenon arises in periodic structures, where vibration waves can propagate freely in pass bands, but attenuate sharply in band gaps [4]. In the open literature,

* Corresponding author.
  E-mail address: dayi@buaa.edu.cn (D. Zhang).

Nomenclature

K	Blade number
k_x	Wavenumber in x direction
k_y	Wavenumber in y direction
k_α	Wavenumber in α direction
$\mathbf{k}$	Wave vector
$\Delta\alpha$	circumferential dimension for unit cell of the cylinder model
Δy	Axial dimension for unit cell of the cylinder model
λ	Propagation constant
ω	Angular frequency
Ω	Nondimensional frequency
L	Length of the structure
Γ	Kinetic energy
t_c	Thickness of the shell
t_{s1}	Width of the circumferential stiffeners
t_{s1}	Width of the axial stiffeners
h_{s1}	Height of the circumferential stiffeners
h_{s2}	Height of the axial stiffeners
R	Radius of the shell
$\mathbf{q}$	Vector for Nodal displacement
$\mathbf{F}$	Vector for Nodal force
$\mathbf{K}$	Stiffness matrix
$\mathbf{M}$	Mass matrix
$\mathcal{K}$	Vibration energy proportion of different directions

characterisation of vibration band gaps in periodic structures, including beams, grids [5], plates [6] and laminated shells [7] has been examined. The vibration characteristics of free modes for a periodically stiffened shell structure with different configurations have also been investigated in Ref. [8]. Mead and his collaborators [9–11] studied different configurations of stiffeners, e.g. circumferential, axial and orthogonal stiffeners. The band-gap characteristic was plotted by the 3D phase constant surface which is the embryo of the 2D dispersion curve used nowadays. Considering the limitation of the early-stage mathematical calculation method and the oversimplification given to a real structure, more accurate methods and models were put forward later to improve the prediction accuracy. The Wave FEM was proposed in Refs. [7,12,13] that was capable of predicting the wave motion in a two-dimensional periodic structure with acceptable accuracy and negligible computational cost. However, only the boundary curvature of the structure was considered in the original Wave FEM, which limits the prediction accuracy on vibration modes. Thus, improvements are imperative for the application of the Wave FEM to more complicated structures, e.g. a periodically stiffened shell, which is studied in this paper.

The open-literature studies mentioned above aid in understanding the periodicity of shell structures from various points of view, however, little attention has been paid to the effect of excitation direction on vibration response, which is significant in engineering applications. For instance, the casing of an aero-engine, which normally features a thin stiffened shell structure, mainly undertakes radial aerodynamic loads due to the rotation of fan blades [14], thus usually showing the radial vibration with a high amplitude. The radial aero dynamical load always features a high frequency with an order of K times as large as the rotation speed, where K refers to the number of blades near to the casing. Moreover, it is quite difficult to get the global band-gap characteristics for the stiffened shell, which implies that specific or local band gaps may need to be defined. Mead [11] figured out that the bending mode band gaps may exist, which provided a strategy to classify the band gaps by directions. Bennet and Accorsi [15] made some attempts by placing capital letters above each pass band to indicate the directions of maximum displacements (radial, axial or tangential). However, the judgement criterion is rather subjective and only suitable for qualitative insight, and the influence of the curvature was also neglected. This means that a quantitative and objective method is required to select the out-of-plane wave modes. Thus, a mode selection approach based on vibration energies associated with different modes is proposed and validated in this paper.

One objective of this article is to propose an improved Wave FEM which can auto-select the mode shapes of interest, thus providing a reference for the practical application of the vibration isolation design for a stiffened shell structure. The out-of-plane mode shapes and high-frequency aero dynamical load in Engineering are of interest, e.g. from 2500 Hz to 4000 Hz. The improved Wave FEM is presented and the optimisation design based on the Genetic algorithm (GA) is adopted, leading to a fan casing with minimum weight and desired band-gap characteristics. Section 2 reviews the relevant wave concepts. Section

3 provides the wave selection method based on Wave FEM and vibration energies of different directions; the viability is verified both for Wave FEM and classic FEM. The optimisation algorithm for interested band gap and minimum weight is described in Section 4. Finally, conclusions are emphasized in Section 5.

2. Wave theory and wave FEM

2.1. Bloch theorem and Brillouin zone

Bloch's theorem was established by Felix Bloch, to depict the electrical conductivity of metals from the viewpoint of quantum mechanics [16]. It was originally invented to describe the motion of electrons in a periodic lattice field, but it was later extended to investigate elastic waves in a structure [5–7]. The joints of any lattice structure in the solid state physics can be envisioned as a collection of lattice points and associated with a set of basic vectors, which can be regarded as particles and position vector in the engineering structure. In a two-dimensional periodic space, the motion of a particle could be expressed as:

$$u(\mathbf{r}) = u_k(\mathbf{r})e^{i\mathbf{k}\cdot\mathbf{r}}, u(\mathbf{r} + \mathbf{R}) = u(\mathbf{r}) \tag{1}$$

where $\mathbf{r}$ is the position vector; $\mathbf{R}$ is the translation vector of a unit periodic cell; $\mathbf{k}$ is the wave vector of the plane wave; $u(\mathbf{r})$ is the wave vibration displacement. $\mathbf{R}$ can be decomposed into basic vectors $\mathbf{a}_i$:

$$\mathbf{R} = n_1\mathbf{a}_1 + n_2\mathbf{a}_2 \tag{2}$$

where n_1 and n_2 are two integers, the integer pair (n_1,n_2) identifies any other periodic cell obtained by n_1 translations along the $\mathbf{a}_1$ direction and n_2 translations along the $\mathbf{a}_2$ direction. A periodic stiffened plate structure and corresponding basic vectors $\mathbf{a}_1$ and $\mathbf{a}_2$ are shown in Fig. 1.

To figure out the physic mechanism and obtain the band gaps in vibration problem, we describe the vibration issue from the wave propagation aspect, which can be easily discussed in the reciprocal lattice. We also use the definitions of wave vector and wave propagation constant μ to explain the mathematical process. The analysis of band gaps always exists in the reciprocal lattice [17]. It is convenient to define the reciprocal lattice in the wave vector space. Through the Fourier transform, the basic vectors of the direct and reciprocal lattice satisfy:

$$\mathbf{a}_i \cdot \mathbf{b}_j = 2\pi\delta_{ij} \tag{3}$$

where $\mathbf{a}_i$ and $\mathbf{b}_j$ denote the basic vectors associated with the direct lattice and the reciprocal lattice, respectively. δ_{ij} is the Kronecker delta function. The reciprocal lattice is also periodic and the unit cell in reciprocal lattice is defined as Brillouin Zone. One can only restrict the wave vector in the first Brillouin Zone to characterise all the band-gaps. In particular, considering the symmetry of the zone, only the edge of the irreducible part needs to be considered to increase the computational efficiency. The typical first Brillouin Zone and its irreducible part of a square planer lattice are shown in Fig. 2, where a is the length of the unit cell in the direct lattice. Considering the irreducible part, only the wavenumbers k_x and k_y in $0\sim\pi/a$ are considered here.
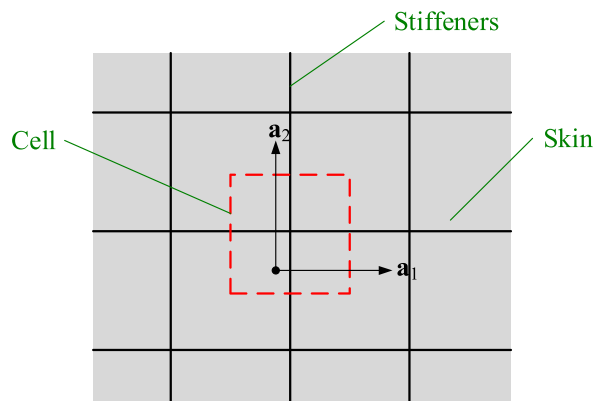

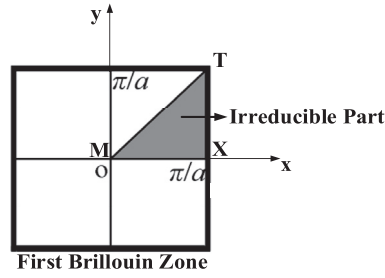**Fig. 1.** The periodic stiffened plate structure.

Fig. 2. Brillouin Zone in two-dimensional space.

2.2. Wave FEM

Wave FEM [7] is an effective method to calculate the band-gap characteristics. The basic concept of Wave FEM comprises following three steps: i) the mass and stiffness matrices of the FE model of a unit cell are obtained by the classical FE method, which can be accomplished by a commercial FE package; ii) the periodic boundaries regarding displacements and forces are applied to the unit cell based on Bloch's Theorem; and iii) the eigenfunction problem is solved to obtain the band-gap characteristics.

The governing equation of the unit cell can be written as:

$$\left(\mathbf{K} - \omega^2 \mathbf{M}\right)\mathbf{q} = \mathbf{F} \tag{4}$$

where the damping matrix is neglected; $\mathbf{K}$ and $\mathbf{M}$ are the stiffness and mass matrices; $\mathbf{q}$ and $\mathbf{F}$ are the nodal displacement and force vectors respectively; ω is the frequency of interest. For the shell structure studied here, it is convenient to describe its deformation in a cylindrical coordinate system. Considering a two-dimensional periodic shell structure, the time harmonic disturbance corresponding to the frequency ω and the nodal displacement of the j_{th} node in a cylindrical coordinate can be expressed as:

$$\mathbf{q}(\mathbf{r}_j, t) = q_j \mathrm{e}^{\left(\mathrm{i}\omega t - k_\alpha \cdot \Delta\alpha - k_y \cdot \Delta y\right)} \tag{5}$$

where q_j is the wave amplitude; k_α and k_y are the projections of the physical wavenumbers in the α and y directions, respectively. The cylinder with a radius of R and a thickness of h is given in Fig. 3 (a), while its unit cell is illustrated in Fig. 3 (b).

As illustrated in Fig. 4, for a two-dimensional periodic structure, the nodes of its unit cell can be partitioned into 9 parts:

$$\mathbf{q} = [\mathbf{q}_i \quad \mathbf{q}_l \quad \mathbf{q}_{lb} \quad \mathbf{q}_{lt} \quad \mathbf{q}_b \quad \mathbf{q}_t \quad \mathbf{q}_r \quad \mathbf{q}_{rb} \quad \mathbf{q}_{rt}]^H \tag{6}$$

where the superscript H denotes the operator of transpose and the subscripts i, l, r, b and t correspond to the internal, left, right, bottom and top nodes.

Using Bloch's theorem, the periodic boundaries can be expressed as:

$$\begin{aligned}
&\mathbf{q}_r = \lambda_\alpha \mathbf{q}_l, \mathbf{q}_t = \lambda_y \mathbf{q}_b, \\
&\mathbf{q}_{lt} = \lambda_y \mathbf{q}_{lb}, \mathbf{q}_{rb} = \lambda_\alpha \mathbf{q}_{lb}, \mathbf{q}_{rt} = \lambda_\alpha \lambda_y \mathbf{q}_{lb}, \\
&\mathbf{F}_r = -\lambda_\alpha \mathbf{F}_l, \mathbf{F}_t = -\lambda_y \mathbf{F}_b, \\
&\mathbf{F}_{rt} + \lambda_\alpha \mathbf{F}_{lt} + \lambda_y \mathbf{F}_{rb} + \lambda_\alpha \lambda_y \mathbf{F}_{lb} = 0
\end{aligned} \tag{7}$$

where λ_α and λ_y satisfy $\lambda_\alpha = \mathrm{e}^{-\mathrm{i}k_\alpha \Delta\alpha}$, $\lambda_y = \mathrm{e}^{-\mathrm{i}k_y \Delta y}$, the nodal displacements and forces can be rearranged as:
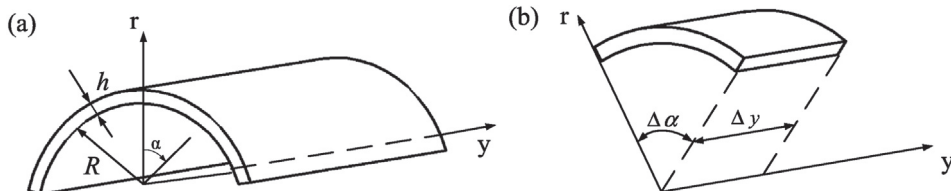

Fig. 3. Illustration of a cylinder model, (a) the isotropic cylinder model and (b) the unit cell.
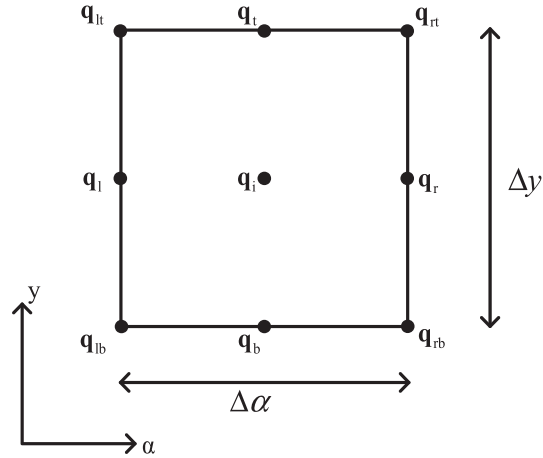
Fig. 4. A two-dimensional unit cell.

$$\mathbf{q} = \begin{bmatrix} \mathbf{q}_i \\ \mathbf{q}_l \\ \mathbf{q}_{lb} \\ \mathbf{q}_b \\ \mathbf{q}_{lt} \\ \mathbf{q}_t \\ \mathbf{q}_r \\ \mathbf{q}_{rb} \\ \mathbf{q}_{rt} \end{bmatrix} = \mathbf{Q}_r \mathbf{q}_{red} = \begin{bmatrix} \mathbf{I} & 0 & 0 & 0 \\ 0 & \mathbf{I} & 0 & 0 \\ 0 & 0 & \mathbf{I} & 0 \\ 0 & 0 & 0 & \mathbf{I} \\ 0 & 0 & \lambda_y\mathbf{I} & 0 \\ 0 & 0 & 0 & \lambda_y\mathbf{I} \\ 0 & \lambda_\alpha\mathbf{I} & 0 & 0 \\ 0 & 0 & \lambda_\alpha\mathbf{I} & 0 \\ 0 & 0 & \lambda_\alpha\lambda_y\mathbf{I} & 0 \end{bmatrix} \begin{bmatrix} \mathbf{q}_i \\ \mathbf{q}_l \\ \mathbf{q}_{lb} \\ \mathbf{q}_b \end{bmatrix} \tag{8}$$

$$\mathbf{Q}_l\mathbf{F} = \begin{bmatrix} \mathbf{I} & 0 & 0 & 0 & 0 & 0 & 0 & 0 & 0 \\ 0 & \mathbf{I} & 0 & 0 & 0 & -\lambda_\alpha^{-1}\mathbf{I} & 0 & 0 & 0 \\ 0 & 0 & \mathbf{I} & 0 & -\lambda_y^{-1}\mathbf{I} & 0 & -\lambda_\alpha^{-1}\mathbf{I} & (\lambda_\alpha\lambda_y)^{-1}\mathbf{I} \\ 0 & 0 & 0 & \mathbf{I} & 0 & -\lambda_y^{-1}\mathbf{I} & 0 & 0 & 0 \end{bmatrix} \begin{bmatrix} \mathbf{F}_i \\ \mathbf{F}_l \\ \mathbf{F}_{lb} \\ \mathbf{F}_b \\ \mathbf{F}_{lt} \\ \mathbf{F}_t \\ \mathbf{F}_r \\ \mathbf{F}_{rb} \\ \mathbf{F}_{rt} \end{bmatrix} = 0 \tag{9}$$

In the combination of Eq. (4), Eq. (8) and Eq. (9), the governing equation for ω or λ_α and λ_y can be determined as:

$$\left(\overline{\mathbf{K}} - \omega^2\overline{\mathbf{M}}\right)\mathbf{q}_{red} = 0 \tag{10}$$

where the reduced stiffness matrix $\overline{\mathbf{K}}$ and the mass matrix $\overline{\mathbf{M}}$ can be calculated using:

$$\overline{\mathbf{K}} = \mathbf{Q}_l\mathbf{K}\mathbf{Q}_r, \overline{\mathbf{M}} = \mathbf{Q}_l\mathbf{M}\mathbf{Q}_r \tag{11}$$

and the nodal displacement matrix $\mathbf{q}_{red}$ is:

$$\mathbf{q}_{red} = [\mathbf{q}_i \quad \mathbf{q}_l \quad \mathbf{q}_{lb} \quad \mathbf{q}_b]^H \tag{12}$$

For a cylinder, due to the closure of its geometry along its circumferential direction, the wavenumber k_α corresponds to the circumferential mode number n, which can only take the integers of 0, 1, 2 …

The computational procedure adopted to calculate the dispersion curves (band structure) for the stiffened shell is as follows.

(1) Select a unit cell of the shell as shown in Fig. 5 (b) and build the FE model in ANSYS.
(2) Classify the nodes of the unit cell according to the rule described in Fig. 4
(3) Rotate the nodal local coordinate (where the FE model is obtained) from the default Cartesian coordinate to the cylindrical coordinate and obtain the mass and stiffness matrices of the unit cell in ANSYS directly.
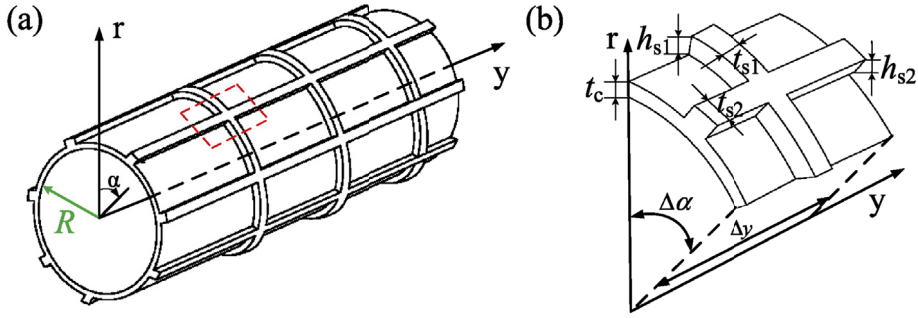
Fig. 5. Numerical models of (a) the orthogonally stiffened cylinder and (b) its unit cell.

(4) Rearrange the mass and stiffness matrices as the order in Eq. (6) by the information we obtained in step (2).
(5) Apply the Wave FEM (Bloch's principle described in Eq. (7)) in MATLAB to the equation of motion for one unit cell and form the eigenvalue problem in Eq. (10).
(6) Solve the resulting eigenvalue problem in for the wave propagation frequencies or the wave propagation constants and construct the dispersion curves.

Above procedure can be applied for all the periodic structures and obtained the band-gap characteristics effectively. Mace [7] presented a specific method based on the Wave FEM for the isotropic cylinder, the difference from the Wave FEM in this paper is the nodal local coordinate for the mass and stiffness matrices. In step (3), Mace obtained the matrices in the default Cartesian coordinate and adopted a simplified coordinate transfer matrix to model the desired curvature. The internal nodes were neglected, thus it can not be used in the complex periodic shell for the accurate wave mode estimation.

3. Wave selection

It is well known that vibration amplitudes of an engineering component are affected by a number of factors, including the excitation frequency, the excitation location, the excitation amplitude and the excitation direction. A shell component in service is more susceptible to out-of-plane vibration, which implies that the excitation direction usually follows the radial direction of the shell structure. This is in particular true for an aero engine casing, which usually experiences out-of-plane vibration due to unstable aerodynamic loads. Therefore, one objective of this study was to achieve out-of-plane vibration modes using the Wave FEM, which was also motivated by improvements on the prediction efficiency.

3.1. Method

In the cylindrical coordinate system, the out-of-plane motion of the shell can be considered to be radial vibration dominated, while the in-plane motions are attributed to longitudinal and torsional vibration.

The stiffened shell comprises two parts, i.e. the uniform shell and stiffeners. As emphasis is placed on the overall vibration of the whole structure, the local vibration of stiffeners needs to be excluded from the overall vibration, since it may disturb the judgement of wave modes. In this wave selection method, vibration energy is divided by the vibration direction and only the shell energy is taken into account for the analysis and judgement, while the vibration performance includes both shell and stiffeners. Thus, the band-gap characteristics exist in the whole stiffened shell. Recalling to section 2, the displacements of the nodes associated with the unit cell can be expressed as:

$$\mathbf{q} = \begin{bmatrix} \mathbf{q}_i & \mathbf{q}_l & \mathbf{q}_{lb} & \lambda_y \mathbf{q}_{lb} & \mathbf{q}_b & \lambda_y \mathbf{q}_b & \lambda_\alpha \mathbf{q}_l & \lambda_\alpha \mathbf{q}_{lb} & \lambda_\alpha \lambda_y \mathbf{q}_{lb} \end{bmatrix}^H \tag{13}$$

which indicates the deformation information of the structure. By removing the vibration associated with the stiffener nodes, the kinetic energy of the shell Γ can be ex pressed by:

$$\Gamma_j = \frac{1}{2} \left[\left(i\omega \mathbf{q}_{sj} \right)^H \mathbf{M}_s \left(i\omega \mathbf{q}_{sj} \right) \right] (j = \alpha, r, y) \tag{14}$$

where the subscripts s represents the shell, α, r and y indicate the circumferential, radial and axial directions, respectively. The contributions by different directions of vibration to the overall kinetic energy can be defined as:

$$\kappa_j = \left| \frac{\Gamma_j}{\Gamma} \right| \times 100\% (j = \alpha, r, y) \tag{15}$$

Accordingly, $\kappa_r > 50\%$ implies that it is an out-of-plane vibration dominated case.

3.2. Verification

The Wave FE model of the orthogonally stiffened cylinder studied here is shown in Fig. 5.

It's originated from the real casing structure of the aero-engine. For the requirement of the manufacture process of the aero-engine, the stiffened casing structure is firstly obtained as a rough cast, and further milling is necessary. The stiffeners are continuously bounded to the skin in the simulation process since the same elements and shared nodes are adopted which match the practical engineering issue well. The specific modelling method is described in the following section 3.2.2.

The geometry parameters of the numerical model are given in Table 1 in a non-dimensional form relative to the shell thickness t_c. Table 1 also gives material parameters used in the wave FE model.

The band-gap characteristics analysis and periodic boundary conditions of the unit cell are originated from the infinite periodic structure. Thus the periodic number is assumed as infinite. However, in the practical engineering, the periodic number is limited to a finite number. The vibration band gap obtained by one unit cell in infinite structure performs as the vibration attenuation of the finite structure in the same frequency range. And the attenuation ability grows with the periodic number. Thus, sufficient periodic number should be guaranteed in the finite structure, to reach the effective vibration isolation. The circumferential and axial periodic number are given at 18 and 8, respectively. The geometric parameters $\Delta\alpha$ and Δy of the unit cell are 20°and 84.7 mm, respectively. Considering the irreducible part of the first Brillouin zone, the circumferential wavenumbers k_α can be restricted at the integers of 0, 1, 2 …, 9.

3.2.1. Wave FEM results

The strong evanescent waves that are present only around the discontinuous points of the structure, such as the excitation points and boundaries are ignored here. The propagation constant λ_y is considered to have a value in the close interval of [0, 1]. The dispersion curve obtained by the Wave FEM for $k_\alpha = 0$ is shown in Fig. 6.

Ω is the non-dimensional frequency defined as $\Omega = \omega/\omega_r$, where:

$$\omega_r = 1/R\sqrt{E/\rho(1 - v^2)} \tag{16}$$

Table 1
Geometry and material parameters of the orthogonally stiffened cylinder.

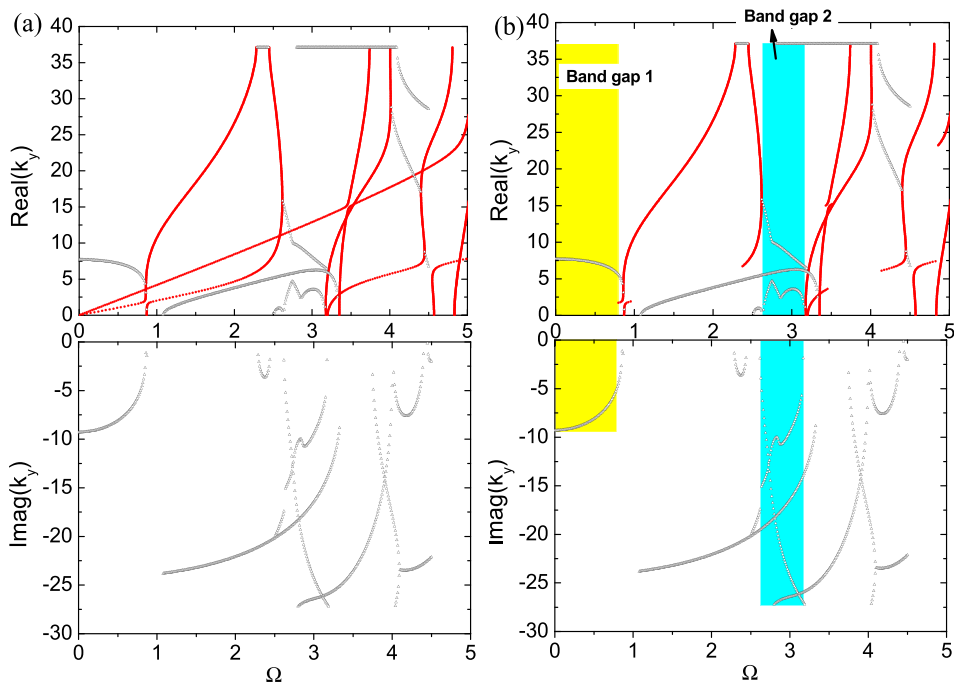| t_c (mm)	H_1 (t_{s1}/t_c)	H_2 (t_{s2}/t_c)	H_3 ($h_{s1,2}/t_c$)	H_4 (R/t_c)	H_5 (Axial period)	H_6 (circumferential period)	P (kg/m^3)	E (GPa)	v
5	4	4	8	150	8	18	7780	206	0.27

Fig. 6. The dispersion curves of the stiffened cylinder (a) without wave mode selection and (b) with wave mode selection.

ω_r is the ring frequency, which is 1094.9 Hz in this example. The dispersion curves obtained before and after the wave mode selection are respectively presented in Fig. 6 (a) and (b). The triangular symbols represent the attenuation waves which correspond to the complex, where dots indicate the propagation waves which correspond to the pure imaginary wave-numbers while the wavenumbers. It can be seen from Fig. 6 (b) that after the wave mode selection there exist two global out-of-plane band gaps in the frequency range of interest. One is located in the low frequency range (LF) at 0–870.1 Hz and the other one is located in the middle-high frequency range (MF/HF) at 2868.5–3470.7 Hz, which are highlighted by band gap 1 and band gap 2 in Fig. 6(b), respectively. Fig. 6(a) also shows that there is not such a global band gap without the wave mode selection, albeit a local band gap may exist between two specific wave modes.

Fig. 7(a) shows the out-of-plane (radial) deformation of the shell, which was retained after the wave selection procedure, while Fig. 7(b) presents the in-plane (circumferential) deformation of the shell, which was eliminated after the wave selection procedure. From the physical point of view, the wave selection method emphasizes the strain energy proportion in different directions, therefore it can figure out the concerned vibration modes according to the actual engineering needs.

3.2.2. ANSYS results

The frequency response (FR) curves of vibration can describe the band-gap characteristics of the finite structure more intuitively. A finite cylindrical shell relating to a real aero-engine fan casing was modelled in the commercial FE package ANSYS. SHELL181 elements are used for developing the wave finite element model which cover the curvature characteristic well. The element is 3D, quadrilateral and four-node shell element with six degrees of freedom on each node, thus having bending and membrane capabilities. It is suitable for analyzing thin and moderately-thick shell structures. The Mindlin-Reissner theory is adopted to describe both the skin and ribs which considers the shear deformation of the structure. However, there are two main assumption and restrict for this element:

1. Shear deflections are included in the element, however, normals to the center plane before deformation are assumed to remain straight after deformation.
2. Transverse shear stiffness of the shell section is estimated by an energy equivalence procedure. The accuracy of this calculation may be adversely affected if the ratio of material stiffness (Young's moduli) between skin and ribs is very high. In our study, only one material is considered.

There were 11520 SHELL181 elements to model both the shell and stiffeners, as shown in Fig. 8(a). The geometric parameters shown in Table 1 were also used in the ANSYS model, and the axial length L is given as 677.23 mm, i.e. 8 periods along the axial direction. The simulation model is isotropic and continuous which matches the practical manufacturing process well. To study the influence caused by the boundary condition of the finite structure, both free-free boundary and free-clamped boundary were considered for two sides of the shell. The harmonic load was applied on all the left-edge nodes of the casing in the radial direction, as Fig. 8(b). The radial displacement responses at two positions, i.e. the middle and right edges of the casing, were taken into account after the harmonic calculation. For the free-clamped boundary, we take the response from the nodes next to the right side.

The FR curves extracted at two positions of the stiffened shell structure under two different boundary conditions are presented in Fig. 9. At the free-clamped boundary condition, all the degrees of right-side nodes are constrained, thus the FR is taken from the near node of the right side. The amplitude variations of these four FR curves demonstrate apparent differences, in particular between these two FR curves extracted at the right edge of the shell. However, there are minor differences between these two boundary conditions regarding the vibration band-gap locations in the frequency domain. They both show a low-frequency band gap at 0–935.5 Hz (Band gap 1 in Fig. 9) and a high-frequency band gap at 2915.2–3465.8 Hz (Band gap 2 in Fig. 9), which were also obtained by the Wave FEM. Thus, good agreements have been observed between the Wave FEM and the ANSYS simulation regarding the band gaps.
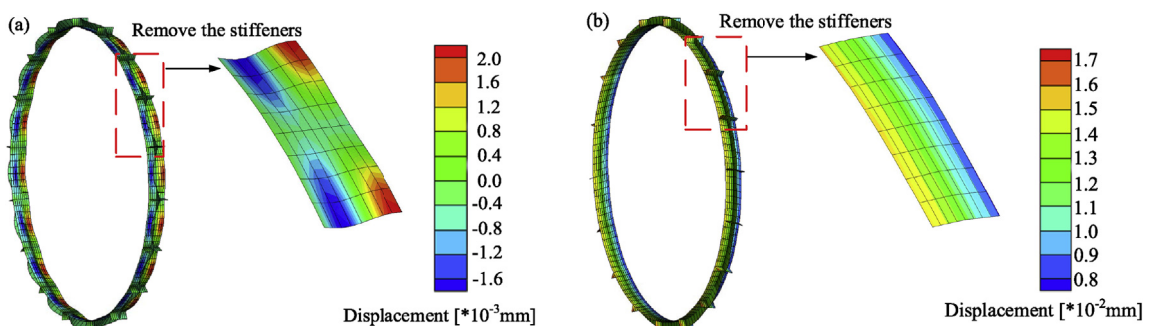

Fig. 7. Shell deformation due to (a) the retained wave modes in radial direction and (b) the removed wave modes in circumferential direction.
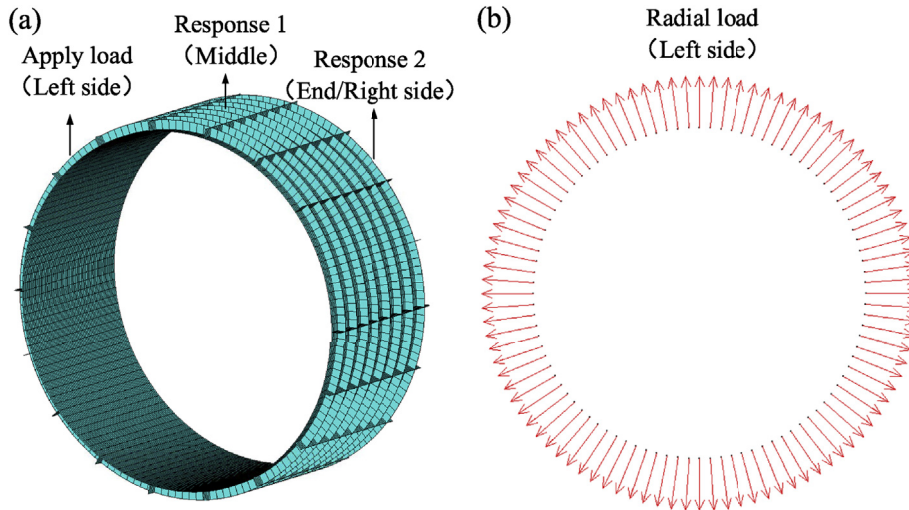
Fig. 8. (a) Finite element model of a periodically stiffened shell structure, and (b) the load applied on the left-edge nodes.
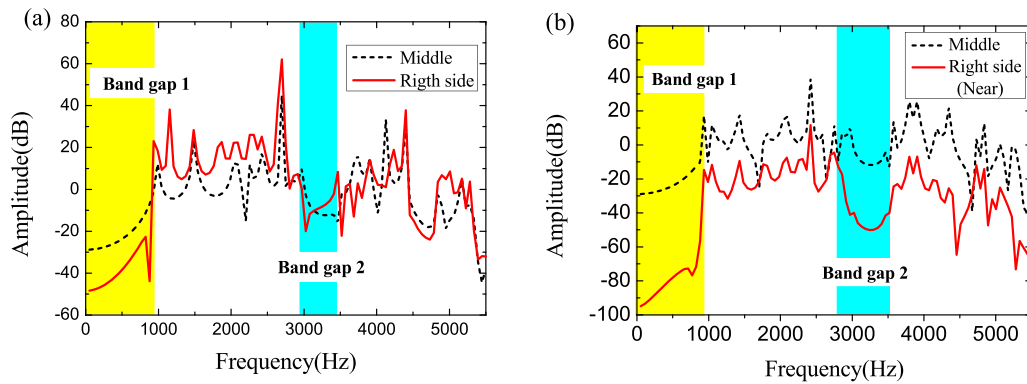

Fig. 9. The frequency response curves for the stiffened shell under (a) free-free boundary and (b) free-clamped boundary.

The contour maps for the out-of-plane strain of specific wave modes under the free-free boundary are given in Fig. 10. Fig. 10 (a) and (c) are the wave modes in the frequency range associated with the band gap 1 and band gap 2, respectively. It can be observed that these two wave modes prevail only near the exciting position. The wave modes out of the band gaps in Fig. 10 (b) and (d) spread throughout the whole structure, hence leading to more severe vibration of the shell in comparison to the aforementioned wave modes both in the band gap1 and band gap 2.

The free mode of the shell was also analyzed in ANSYS. Fig. 11 shows the displacement contour map for the first out-of-plane vibration mode at the natural frequency of 926.6 Hz, which is quite close to the upper cut-off frequency of the gap band 1.

Wave propagation characteristics underlie the vibration and acoustic performance of a structure. The related rising research field concerning the periodic structures is a typical issue mainly based on the wave theory, the key of wave theory is the Bragg scattering of the vibration wave happens near the periodic boundary, thus the vibration in the specific frequency range can be isolated. The wave-based methods can, at least in theory, lead to the same result for a structural dynamical problem as the conventional mode based methods [18], and this equivalence is termed "wave-mode duality" in the literature [19–21].

In comparison to the traditional mode-based method, the wave-based method shows advantages regarding treatments of mid- and high-frequency problems. The latter can remarkably reduce the problem dimensions, achieve the band-gap features and conveniently explain corresponding physical mechanisms.

4. Numerical optimisation

The wave selection strategy proposed above was further employed to investigate the optimisation design of a periodically stiffened shell structure, in the combination of the classical genetic algorithm.
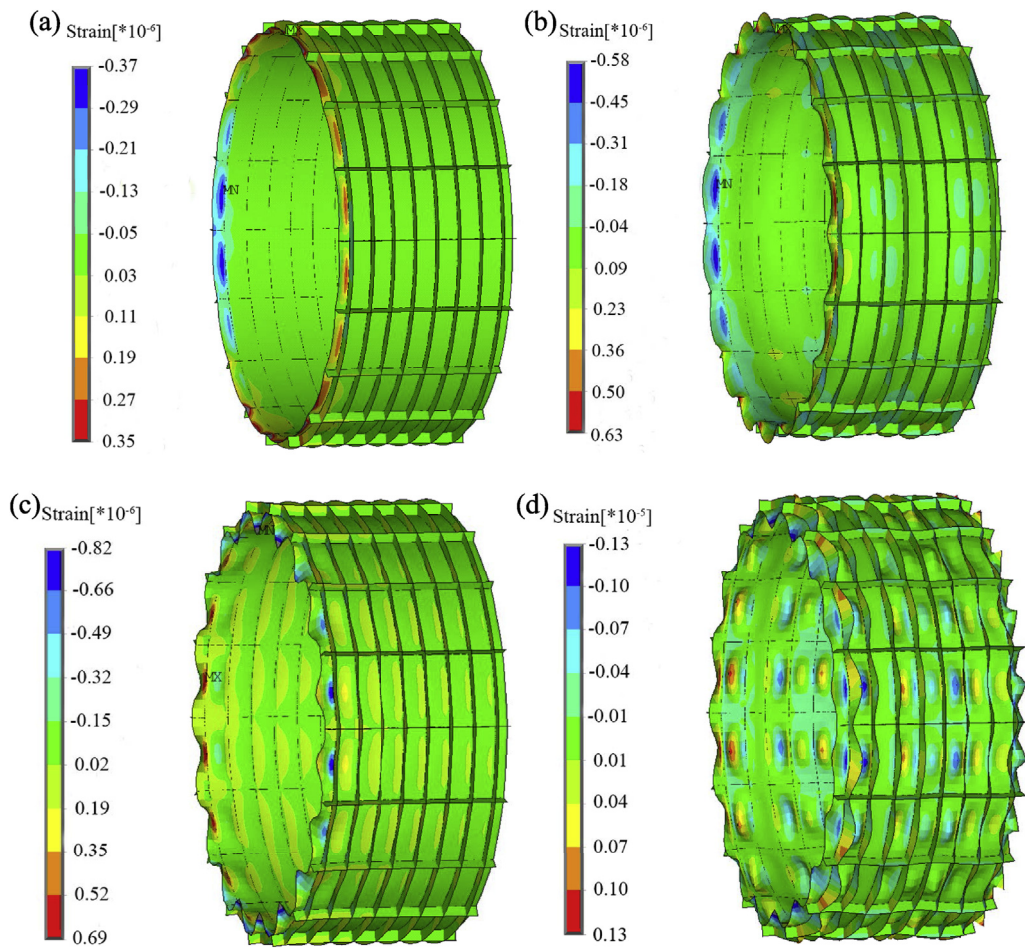
Fig. 10. The strain distribution of the stiffened shell under the free-free boundary condition at (a) 550.1 Hz, (b) 1705.3 Hz, (c) 3245.2 Hz and (d) 4180.7 Hz.
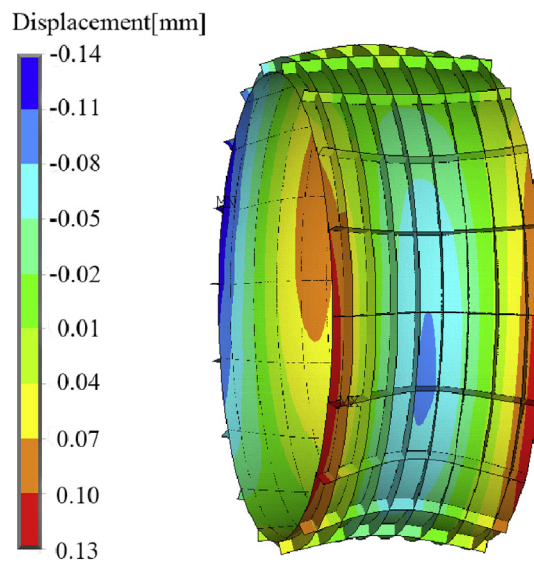

Fig. 11. The first out-of-plane vibration mode of the shell ($k_z = 0$, 926.6 Hz).

4.1. Optimisation parameters and aims

The optimised body is the stiffened shell structure as studied in Section 3 and shown in Fig. 5. The geometric parameters of the periodic structure are given above in.

Table 1, where $H1$, $H2$, $H3$, $H4$, $H5$ and $H6$ are the optimisation parameters. The selection and design of the optimisation parameters are based on the above calculation and simulation.

This optimisation problem is a typically multi-objective optimisation problem. Three main aims were set in this optimisation procedure. AimI: the interested frequency range needs to be covered in the band gap. AimII: the median frequencies of the band gap and the desired frequency range are close. Aim III: the minimum mass of the whole structure is obtained.

4.2. Optimisation algorithm (genetic algorithm)

Since all the parameters considered in the optimisation design influence and interact with one another, the optimisation design needs to take into account the relations amongst the parameters and achieve the vibration isolation in a relatively wide frequency range. Genetic algorithm was adopted for the optimisation design.

Genetic algorithms (GA) is an optimisation algorithms developed from the process of natural evolution and selection. It's commonly used to generate high-quality solutions to optimise and search problems by relying on bio-inspired operators such as mutation, crossover and selection [22]. With the random and global search characteristics, GA makes it almost impossible to fall into local optimum. And there is no restrict of the derivative and continuity of optimisation function. It is appropriate to deal with the multi-objective optimisation problem and may reduce the iteration times enormously. The flow chart of the optimisation procedure is shown in Fig. 12.

4.3. Band-gap design

Considering the frequency range between the cruising and the maximum speed of the real aero-engine, the rotation speed is between 77 Hz and 88 Hz. The number of blades is 38. The blade passing frequency is equal to the rotation speed times blade number, thus the desired band gap is expected to be between 2926 Hz and 3344 Hz.

4.3.1. Optimisation parameters and objective function

Considering the manufacture errors, the allowable tolerance in engineering and the qualitative change in the band gaps, the variations of the geometric parameters H_1, H_2 and H_3 were assumed to be 0.5 times as large as the shell thickness. The
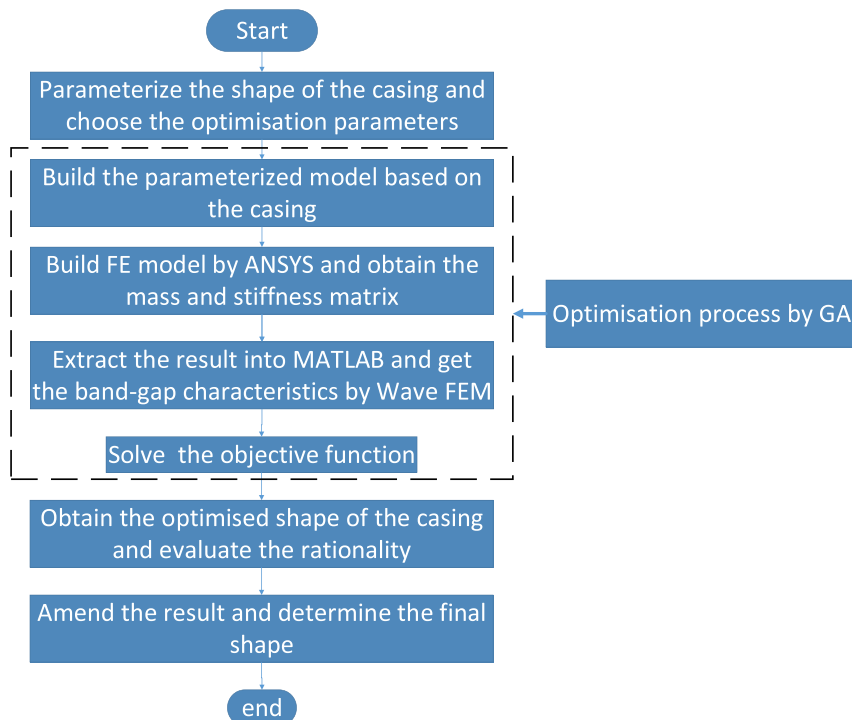

Fig. 12. The flow chart of the optimisation procedure by GA.

Table 2
The optimised parameters of the casing.

H_1 (t_{s1}/t_c)	H_2 (t_{s2}/t_c)	H_3 ($h_{s1,2}/t_c$)	H_4 (R/t_c)	H_5 (Axial period)	H_6 (circumferential period)
3	5.5	9.5	170	5	21

ranges of the six optimisation parameters H_1, H_2, H_3, H_4, H_5 and H_6 are at 1–6, 1–6, 1–15, 150–200, 5–8 and 20–24 respectively. The thickness of the shell, t_c, and the axial length of the casing, L, were fixed at 5 mm and 677.22 mm, respectively.

By introducing the weight coefficient W_i ($i = 1, 2$), we can convert this multi-objective optimisation problem into a single-objective optimisation problem. The subscript i indicate aim 1 and aim 2. Thus the objective function is:

$$Obj = W_1[(x_1 - lower) + (upper - x_2)] + W_2 \times abs[(x_1 + x_2) - (upper + lower)] \tag{17}$$

where x_1 and x_2 are the lower and upper bound respectively; *upper* and *lower* are the desired frequencies. In this case, *upper* = 3344 Hz and *lower* = 2926 Hz.

To improve the calculation efficiency and accuracy, the objective function only includes the first two optimisation aims (Aim I and Aim II). A set of results is obtained and defined as result_0. However Aim I can not be satisfied completely as the shortage of the optimisation algorithm. Considering AimI is more critical and obligatory for the practical engineering cases, further optimisation is still needed to search within the result_0. Consequently the restriction conditions: $x_1 \geq lower$ and $x_2 \leq upper$ need to be added, and then the result_1 can be reached. Finally, the aim of minimizing the whole mass of the structure (Aim III) is achieved by searching amongst the result_1 following the above optimisation procedure, and the final result can own the minimal mass among the result_1.

4.3.2. Results

The optimised results are shown in Table 2. The corresponding band-gap frequency range is 2657.2–3666.1 Hz, which covers the frequency range of interest, i.e. 2926–3344 Hz. The minimum mass of the casing given by the optimisation algorithm is 437.3 kg.

4.4. Simulation and verification

The FE model of the cantilever fan casing structure was realized using 8400 SHELL181 elements in ANSYS. The free-clamped boundary was applied to the structure. The frequency response of the right side of the structure is given in Fig. 13.

The bar in Fig. 13 indicates the theoretical band-gap frequency range, which is clearly captured by two large vibration-amplitude drops. An interesting phenomenon that can be observed in Fig. 13 is that one peak appears in the FR curve at 3300 Hz. The free modal analysis indicates that it corresponds to the natural frequency of the structure. The existence of band gaps can not eliminate the resonance, i.e. resonance in the band gaps is inevitable. In spite of this, the band gap can still degrade the influence due to the resonance, and the degradation extent increases with more periods.
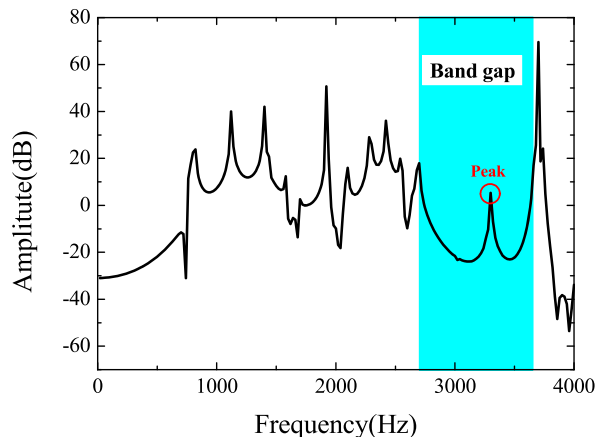

Fig. 13. The FR curve of the optimised casing.

5. Conclusions

An improved Wave FEM method has been put forward by considering the boundary and the internal nodes accurately in a cylindrical coordinate and by introducing a wave selection idea. Therefore the vibration band-gap characteristics of the stiffened periodic shell can be achieved efficiently. The optimisation method GA was adopted for the design of a fan casing. The configuration parameters are optimised so that the wave does not span across the concerned broad frequency range. The vibration isolation method developed in this article can provide a reference for the practical application on the optimisation design of the stiffened shells.

Acknowledges

References

[1] C.A.I. Xianxin, X. Xinhong, W.A.N.G. Tao, W.U. Zhiqing, Optimization design of a fan casing for reducing vibration, J. Aero. Power 25 (2010) 396–401, https://doi.org/10.13224/j.cnki.jasp.2010.02.012.

[2] C. Li, H. She, Q. Tang, B. Wen, The effect of blade vibration on the nonlinear characteristics of rotor–bearing system supported by nonlinear suspension, Nonlinear Dynam. 89 (2017) 987–1010, https://doi.org/10.1007/s11071-017-3496-z.

[3] D. Zhang, J. Fu, Q. Zhang, J. Hong, An effective numerical method for calculating nonlinear dynamics of structures with dry friction: application to predict the vibration response of blades with underplatform dampers, Nonlinear Dynam. 88 (2017) 223–237, https://doi.org/10.1007/s11071-016-3239-6.

[4] Z. Guo, M. Sheng, J. Pan, Flexural wave attenuation in a sandwich beam with viscoelastic periodic cores, J. Sound Vib. 400 (2017) 227–247, https://doi.org/10.1016/j.jsv.2017.04.016.

[5] A.S. Phani, J. Woodhouse, N.A. Fleck, Wave propagation in two-dimensional periodic lattices, J. Acoust. Soc. Am. 119 (2006) 1995–2005, https://doi.org/10.1121/1.2179748.

[6] J. Wang, G. Wang, J. Wen, X. Wen, Flexural vibration band gaps in periodic stiffened plate structures, Mechanika 18 (2012) 186–191, https://doi.org/10.5755/j01.mech.18.2.1557.

[7] E. Manconi, B.R. Mace, Wave characterization of cylindrical and curved panels using a finite element method, J. Acoust. Soc. Am. 125 (2009) 154–163, https://doi.org/10.1121/1.3021418.

[8] C.H. Hodges, J. Power, J. Woodhouse, The low frequency vibration of a ribbed cylinder, Part 2: observations and interpretation, J. Sound Vib. 101 (1985) 237–256, https://doi.org/10.1016/S0022-460X(85)81218-9.

[9] D.J. Mead, N.S. Bardell, Free vibration of a thin cylindrical shell with periodic circumferential stiffeners, J. Sound Vib. 115 (1987) 499–520.

[10] D.J. Mead, N.S. Bardell, Free vibration of a thin cylindrical shell with discrete axial stiffeners, J. Sound Vib. 111 (1986) 229–250, https://doi.org/10.1016/S0022-460X(86)80159-6.

[11] N.S. Bardell, D.J. Mead, Free vibration of an orthogonally stiffened cylindrical shell, part II: discrete general stiffeners, J. Sound Vib. 134 (1989) 55–72, https://doi.org/10.1016/0022-460X(89)90736-0.

[12] J.M. Renno, B.R. Mace, Calculating the forced response of cylinders and cylindrical shells using the wave and finite element method, J. Sound Vib. 333 (2014) 5340–5355, https://doi.org/10.1016/j.jsv.2014.04.042.

[13] Y. Waki, B.R. Mace, M.J. Brennan, Numerical issues concerning the wave and finite element method for free and forced vibrations of waveguides, J. Sound Vib. 327 (2009) 92–108, https://doi.org/10.1016/j.jsv.2009.06.005.

[14] L.C. Gong, Aircraft Engine Design, first ed., Aviation Industry Press, Beijing, 2001.

[15] M.S. Bennett, M.L. Accorsi, Free wave propagation in periodically ring stiffened cylindrical shells, J. Sound Vib. 171 (1994) 46–66.

[16] A. Bloch, M.Valiron's Theorems on Integer Functions and Theory of Uniformity, Annals of the Faculty of Sciences of Toulouse, 1925. http://afst.cedram.org/item?id=AFST_1925_3_17__1_0.

[17] L. Brillouin, Wave Propagation in Periodic Structures: Electric Filters and Crystal Lattices, McGraw-Hill Book Company, Inc., New York, 1953.

[18] Y. Fan, Multi-scale Approaches for the Vibration and Energy Flow through Piezoelectric Waveguides: Simulation Strategies, Control Mechanisms and Circuits Optimization, Central school of Lyon, 2016.

[19] X.Q. Wang, R.M.C. So, K.T. Chan, Resonant beam vibration: a wave evolution analysis, J. Sound Vib. 291 (2006) 681–705, https://doi.org/10.1016/j.jsv.2005.06.030.

[20] R.S. Langley, Some perspectives on wave-mode duality in SEA, in: Proc. IUTAM Int. Symp. Stat. Energy Anal., 1997, pp. 1–12.

[21] D.J. Mead, Waves and modes in finite beams: application of the phase-closure principle, J. Sound Vib. 171 (1994) 695–702, https://doi.org/10.1006/jsvi.1994.1150.

[22] M. Mitchell, An introduction to genetic algorithms, Comput. Math. Appl. 32 (1996) 133, https://doi.org/10.1016/S0898-1221(96)90227-8.